https://doi.org/10.46861/bmp.33.001 PŮVODNÍ PRÁCE/ORIGINAL PAPER

Study of phosphate and sulphate association from the Mine No. 6 “Exi” in the Lavrion mining district (Greece): chemistry and PXRD data

Luboš Vrtiška[1)]*, Ivan Prachař[2)], Radana Vrtišková[1)] and Zdeněk Dolníček[1)]

[1)]*Department of Mineralogy and Petrology, National Museum, Cirkusová 1740, 193 00 Praha 9 - Horní Počernice, Czech Republic; *e-mail: lubos.vrtiska@nm.cz*
[2)]*Náchodská 955/38, 193 00 Praha - Horní Počernice, Czech Republic*

Vrtiška L, Prachař I, Vrtišková R, Dolníček Z (2025) Study of phosphate and sulphate association from the Mine No. 6 “Exi” in the Lavrion mining district (Greece): chemistry and PXRD data. Bull Mineral Petrolog 33(1): 1-13. ISSN 2570-7337

Abstract

A large number of supergene minerals has been identified in the Lavrion mining district (Greece). The dominant part belongs to the group of arsenates or sulphates. The substitution of phosphorus for arsenic or the occurrence of phosphates is relatively rare at this mining district. The new occurrence of the association of supergene phosphates including phosphosiderite, mitridatite, jahnsite-(NaFeMg), fluorapatite and collinsite, in association with minerals of the alunite group, jarosite and natrojarosite in the Mine No. 6 “Exi” is therefore unique. A study of the chemical composition of these minerals and PXRD data of selected minerals are presented in this publication.

Key words: *jarosite-natrojarosite solid solution, collinsite, jahnsite-(NaFeMg), phosphosiderite, mitridatite, fluorapatite, phosphate occurrence, chemical composition, PXRD data, Mine No. 6 “Exi“, Lavrion, Greece*

Received 30. 4. 2025; accepted 20. 6. 2025

Introduction

The Lavrion mining district is a part of the Lavreotiki municipality on the southeasternmost tip of the Attica peninsula in Greece. In ancient times, it represented one of the world’s largest centers of silver mining. Mining of silver and other ores took place there with interruptions from the transitional period from the Neolithic to the Bronze Age (around 3200 BC) until the middle of the last century (see https://whc.unesco.org/en/tentativelists/5857/). The Lavrion area is still in the center of interest of mineralogists, archaeologists and those interested in the history of mining. Since 2023, the Lavrion mining district has been part of the Lavreotiki UNESCO Global Geopark (see https://geoparklavreotiki.gr/). The history, geology and mineralogy of Lavrion was first described in the now “classic” work of Marinos and Petrascheck (1956). Since then, a number of scientific studies has been published as well as articles in popular collector magazines devoted to the geology and mineralogy of this deposit. Voudouris et al. (2021) set out to expand on previous work and summarize the current state of knowledge on geology, mineralization, and the supergene mineralogy of the Lavrion deposit.

The Lavrion deposit comprises five genetically-related but different styles of mineralization, containing the highest number of different elements of any known mining district. These five types include (a) porphyry Mo-W, (b) Fe-Cu-Bi-Au skarn, (c) high-temperature carbonate replacement (skarn-free) Pb-Zn-Cu-Ag-Au mineralization, and (d, e) Pb-Zn-Ag-Au vein and breccia. The local geology, tectonic, and magmatic activity were fundamental factors in determining how and when the mineralization formed.

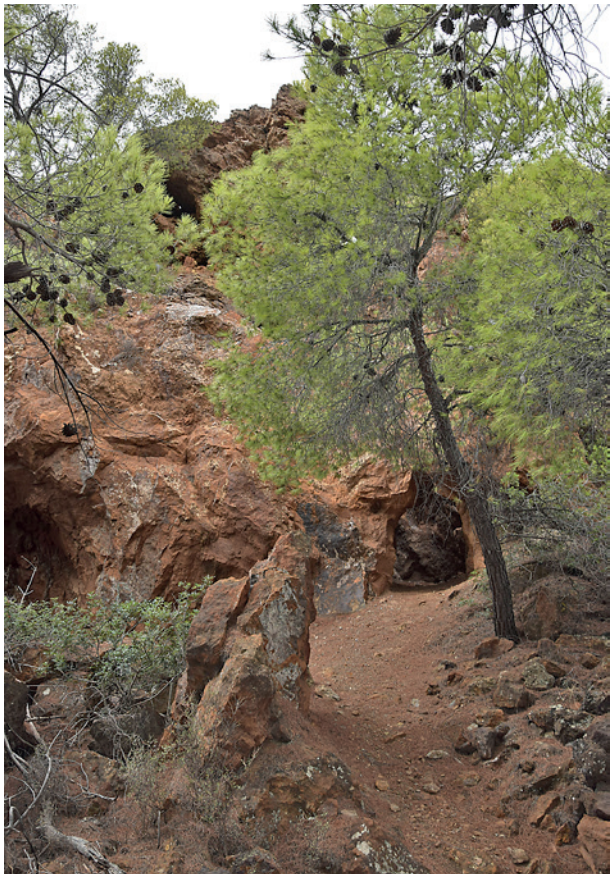

Fig. 1 *Northern entrance to the Mine no. 6 „Exi“ in 2023. Photo by I. Prachař.*

Fig. 2 *I. Prachař at the place of finding the studied mineralization in 2023. Photo by I. Prachař.*

Fig. 3 *Dark and light pink aggregates of phosphosiderite. FOV (field of view) 1.9 mm. Photo by L. Vrtiška.*

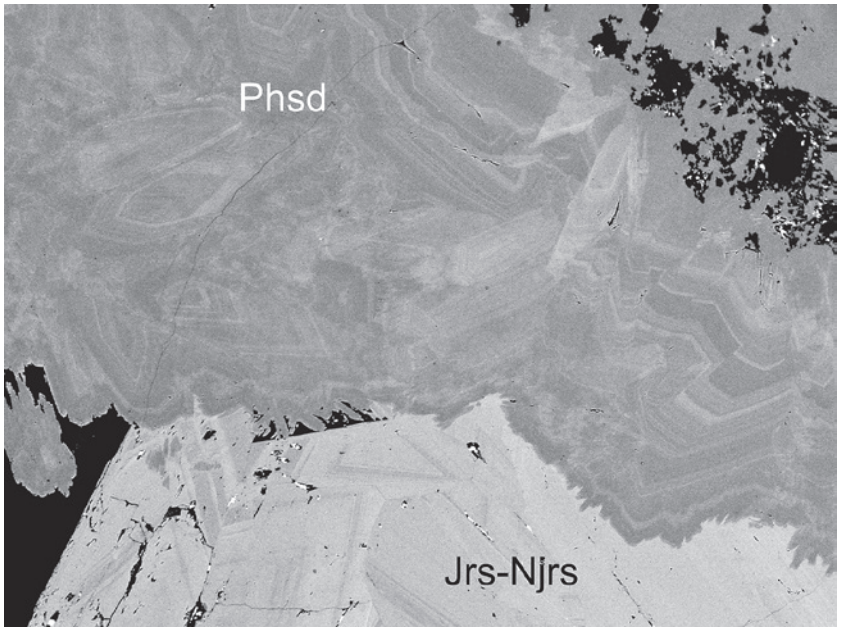

Fig. 4 *Oscillatory compositional zoning of phosphosiderite (Phsd) and jarosite-natrojarosite (Jrs-Njrs). Lighter zones in phosphosiderite are As-rich, lighter zones in jarosite-natrojarosite are K-rich. FOV 1.7 mm. BSE photo by Z. Dolníček.*

Other key factors, such as the rise and the fall of sea level, which resulted from climate change over the last million years, were also of major importance for the subsequent surface oxidation that created an unmatched diversity of supergene minerals at Lavrion (Voudouris et al. 2021). Almost 700 mineral species are known from this mining district to date, of which Lavrion is the type locality for 23 of them (www.mindat.org; March 2025). However, only a few of the mineral species found belong to the group of phosphates.

An interesting association of phosphates and sulphates represented by phosphosiderite, jahnsite-(NaFeMg), collinsite, fluorapatite, mitridatite and minerals of the jarosite group was recently found in Mine No. 6. “Exi“ (Fig. 1). The study of these samples is the subject of this paper.

Occurrence

The studied samples were found by one of the authors of this study (IP) in the Mine No. 6 „Exi“ (GPS: 37.680890N, 24.017390E) in 2023 as part of a stone wall nearby the northern entrance (Fig. 1, 2). This mine belongs to the mining area of Agrileza and is located about 5 km south of the village of Agios Konstantinos (Kamariza). Macroscopic specimens of fluorapatite have been reported from this mine by Rieck et al. (2018). Fluorapatite is characterized as colorless to white spherical aggregates, where spheres consist of sharp, radially oriented hexagonal crystals, grown on well-formed jarosite. The analysis showed that fluorapatite contains a small component of carbonate. The same authors also mention the occurrence of collinsite from this mine.

Experimental

Color microphotographs were taken using a Nikon SMZ25 microscope with a Nikon DS-Ri2 digital camera and the image assembling function using NIS Elements AR version 4.20.

Powder X-ray diffraction data (PXRD) were measured by Bruker D8 Advance diffractometer (National Museum, Prague) with a solid-state 1D LynxEye detector (width 2.05°) using Cu*K*α radiation and operating at 40 kV and 40 mA. The powder patterns were collected using Bragg–Brentano geometry in the range 5 - 70° 2θ, in 0.01° steps with a counting time of 8 s per step. The X-ray powder diffraction data were processed using the program HighScore Plus, where the profile fitting was done using a Pseudo-Voigt profile shape function corrected for asymmetry (full-axial model). Obtained positions of the diffraction maxima were used for the refinement of the unit-cell parameters by the Celref program of the LMGP suite for Windows (Laugier, Bochu 2011), an algorithm based on least-squares method.

The chemical composition of studied minerals was determined on polished and carbon-coated fragments

Table 1 *X-ray powder diffraction data of phosphosiderite from Lavrion*

h	*k*	*l*	d_{obs}	I_{obs}	d_{calc}	*h*	*k*	*l*	d_{obs}	I_{obs}	d_{calc}	*h*	*k*	*l*	d_{obs}	I_{obs}	d_{calc}
0	2	0	4.907	72	4.905	0	2	3	2.4986	2	2.5001	2	4	1	1.7651	10	1.7647
1	1	0	4.686	100	4.683	-1	1	3	2.4809	1	2.4795	3	0	1	1.7369	2	1.7374
-1	0	1	4.572	30	4.569	2	1	1	2.4591	9	2.4600	-3	1	1	1.7169	6	1.7176
1	0	1	4.529	6	4.527	-1	3	2	2.3527	3	2.3541	1	5	2	1.6929	2	1.6939
0	0	2	4.360	94	4.359	1	3	2	2.3424	14	2.3424	-2	4	2	1.6711	18	1.6716
1	1	1	4.111	23	4.110	2	0	2	2.2640	7	2.2633	1	0	5	1.6522	4	1.6521
0	1	2	3.998	1	3.983	1	2	3	2.2554	14	2.2557	0	6	0	1.6362	9	1.6350
1	2	0	3.611	44	3.609	1	4	0	2.2277	6	2.2279	-2	2	4	1.6034	1	1.6028
-1	2	1	3.344	9	3.343	0	0	4	2.1800	4	2.1795	2	5	0	1.5803	5	1.5800
0	2	2	3.258	<1	3.258	0	3	3	2.1721	5	2.1722	-2	5	1	1.5559	4	1.5564
-1	1	2	3.207	6	3.206	1	4	1	2.1566	<1	2.1563	1	6	1	1.5375	3	1.5377
-1	2	2	2.788	86	2.790	0	1	4	2.1278	14	2.1276	2	4	3	1.5288	6	1.5282
1	2	2	2.771	7	2.770	-2	2	2	2.0723	4	2.0709	-3	1	3	1.5046	2	1.5049
2	0	0	2.666	8	2.665	-2	3	1	2.0144	19	2.0139	3	1	3	1.4912	6	1.4913
-1	3	1	2.657	6	2.659	0	2	4	1.9911	4	1.9917	0	0	6	1.4532	1	1.4530
2	1	0	2.5719	36	2.5719	1	5	0	1.8407	4	1.8412	3	4	0	1.4390	3	1.4388
1	0	3	2.5408	10	2.5403	2	2	3	1.8153	13	1.8152	0	2	6	1.3924	5	1.3932

Table 2 *Unit-cell parameters of phosphosiderite (for monoclinic space group P2 1/n)*

	this paper	Fanfani, Zanazzi (1966)
a [Å]	5.3305(8)	5.330(3)
b [Å]	9.8098(15)	9.809(4)
c [Å]	8.7185(12)	8.714(5)
β [°]	90.61(5)	90.60(12)
V [Å^3]	455.9(1)	455.56

Table 3 *Chemical composition of phosphosiderite from Lavrion (wt. %)*

	1	2	3	4	5	6	7	8	9	10	11	12	13	14
Fe_2O_3	41.73	42.46	47.64	42.99	49.04	48.81	49.12	49.11	49.52	48.65	47.21	47.34	49.39	47.51
Al_2O_3	0.00	0.00	0.00	0.00	0.00	0.00	0.13	0.18	0.00	0.21	0.00	0.07	0.09	0.00
P_2O_5	31.39	33.45	38.41	34.28	42.04	40.85	42.19	42.79	42.66	43.25	41.72	43.62	45.12	44.91
As_2O_5	13.51	11.12	8.78	7.66	5.22	5.00	3.92	3.32	2.80	2.51	1.82	1.71	1.47	0.73
SO_3	0.21	0.20	0.10	0.31	0.00	0.13	0.00	0.00	0.35	0.00	0.23	0.12	0.00	0.17
H_2O*	20.27	20.56	22.30	19.94	22.98	22.36	22.65	22.76	22.69	22.74	21.85	22.74	23.37	23.11
total	107.11	107.79	117.23	105.18	119.28	117.15	118.01	118.16	118.02	117.36	112.83	115.60	119.44	116.43
Fe	0.929	0.932	0.964	0.973	0.963	0.985	0.979	0.973	0.985	0.965	0.975	0.940	0.954	0.928
Al	0.000	0.000	0.000	0.000	0.000	0.000	0.004	0.006	0.000	0.007	0.000	0.002	0.003	0.000
Σ	0.929	0.932	0.964	0.973	0.963	0.985	0.983	0.979	0.985	0.972	0.975	0.942	0.957	0.928
P	0.786	0.826	0.875	0.873	0.929	0.927	0.946	0.954	0.954	0.965	0.969	0.974	0.980	0.987
As	0.209	0.170	0.123	0.120	0.071	0.070	0.054	0.046	0.039	0.035	0.026	0.024	0.020	0.010
S	0.005	0.004	0.002	0.007	0.000	0.003	0.000	0.000	0.007	0.000	0.005	0.002	0.000	0.003
Σ	1.000	1.000	1.000	1.000	1.000	1.000	1.000	1.000	1.000	1.000	1.000	1.000	1.000	1.000
H_2O	2.000	2.000	2.000	2.000	2.000	2.000	2.000	2.000	2.000	2.000	2.000	2.000	2.000	2.000

Apfu on the base P+As+S = 1; H_2O* contents were calculated on the basis of ideal content of $2H_2O$.

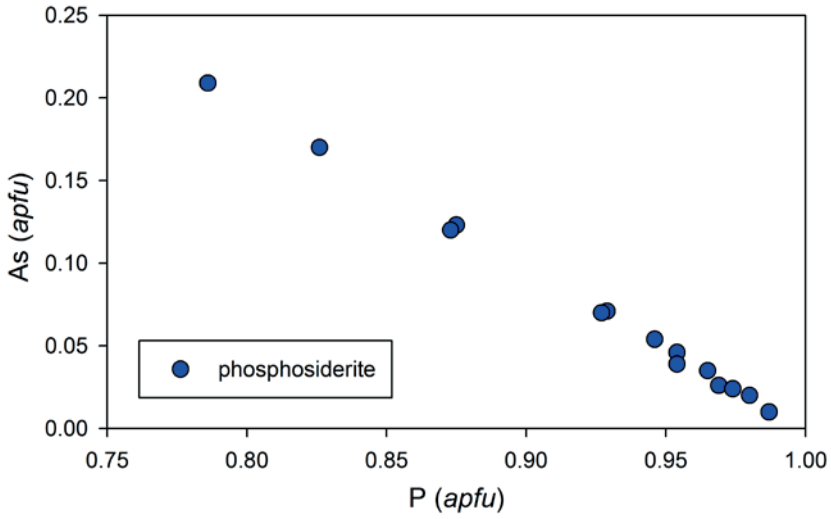

Fig. 5 *Graph of P vs. As (apfu) contents on the basis of P+As+S = 2 apfu for phosphosiderite from Lavrion.*

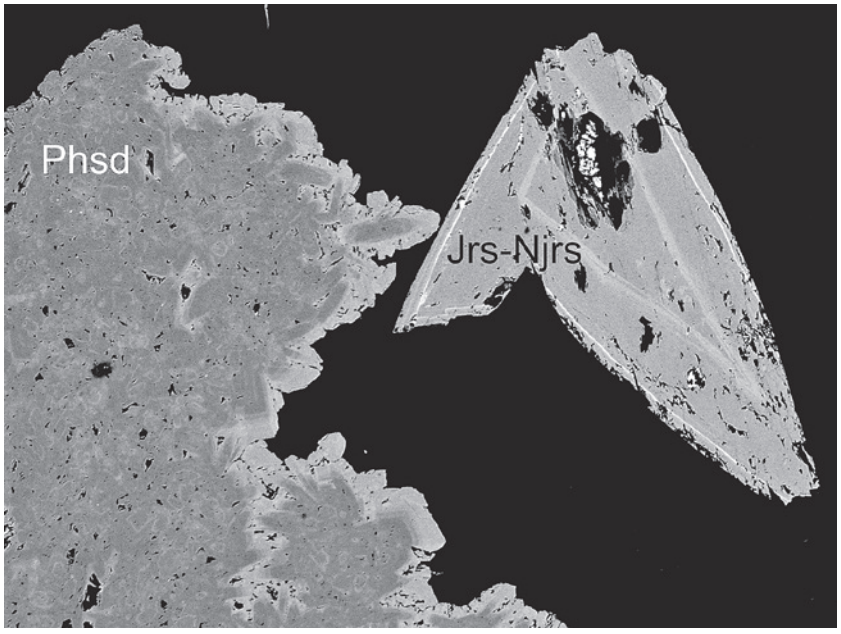

Fig. 6 *Zonality of phosphosiderite (Phsd) and jarosite-natrojarosite. Lighter zones in phosphosiderite are As-rich, lighter zones in jarosite-natrojarosite (Jrs-Njrs) are K-rich. FOV 1.5 mm. BSE photo by Z. Dolníček.*

Fig. 7 *Light pink crystals of phosphosiderite with brown crystals of jarosite-natrojarosite. FOV 6 mm. Photo by L. Vrtiška.*

mounted in an epoxy cylinder using a Cameca SX 100 electron microprobe (EPMA; National Museum, Prague). The instrument was operated in wavelength-dispersive mode at accelerating voltage of 15 kV, beam current of 10 nA, and beam diameter of 4 μm for fluorapatite, and beam current of 5 nA and beam diameter of 5 μm for other minerals. The following X-ray lines and standards were selected; *K*α lines: Na (albite), Al, K (sanidine), Mg (diopside), P, Ca (apatite), Fe (hematite), S (celestite), Zn (ZnO), F (LiF); *L*α lines: As (clinoclase). Contents of Si, Mn, Sr, Cl, Cu, N, V, Cr, Pb, Ba, Ce, La and Nd were below detection limits (mostly ~0.05 - 0.10 wt. %). Counting times were 10 - 20 s on peak and half of this time for each background position. The raw intensities were converted to concentrations automatically using PAP (Pouchou, Pichoir 1985) matrix-correction algorithm. The H_2O content was calculated by stoichiometry of ideal formulas.

Results

The samples are composed of massive light pink phosphosiderite mixed with ochre-colored jarosite-natrojarosite and quartz, in whose cavities and fissures crystals of the studied minerals occur. The minerals in this section are arranged according to observed genetic relationships from the oldest to the youngest one.

Phosphosiderite

Phosphosiderite $FePO_4 \cdot 2H_2O$ forms tabular translucent vitreous dark pink crystals up to 1.5 mm in size and light pink spherical aggregates up to 1 mm in size in the cavities (Fig. 3).

The X-ray powder data of phosphosiderite from Lavrion (Table 1) are consistent with published data for this mineral species (Fanfani, Zanazzi 1966). The refined unit-cell parameters, compared with published data, are given in Table 2.

Phosphosiderite shows oscillatory compositional zoning in the BSE image (Fig. 4), which is primarily caused by the high extent of AsP_{-1} substitution (Table 3; Fig. 5) in the tetrahedral position (0.77 - 0.99 *apfu* P, 0.01 - 0.21 *apfu* As). This type of incorporation of As^{5+} into phosphosiderite was described by Bolanz et al. (2016) as strengite/scorodite-like arrangement. Minor contents of S were also detected at this position (up to 0.01 *apfu*). The highest As contents were found in the peripheral zones of the crystals (Fig. 6). In the cationic position, only low levels of Al (metavariscite component; up to 0.01 *apfu*) were detected in addition to Fe.

Table 4 *Chemical composition of jarosite-natrojarosite from Lavrion (wt. %)*

	jarosite						**jarosite-natrojarosite**				**natrojarosite**					
	1	2	3	4	5	6	1	2	3	4	1	2	3	4	5	6
Na_2O	0.00	0.00	0.09	0.18	0.15	0.72	2.75	2.56	2.75	2.65	5.88	5.83	5.66	5.55	5.29	5.21
K_2O	8.79	8.46	8.88	8.99	8.11	7.93	5.44	4.88	4.45	4.53	0.06	0.13	0.17	0.37	0.85	1.06
CaO	0.00	0.05	0.00	0.00	0.06	0.00	0.00	0.00	0.00	0.05	0.00	0.00	0.00	0.00	0.06	0.13
Fe_2O_3	48.05	47.42	47.23	46.71	47.02	47.72	47.37	47.05	48.58	47.86	49.14	49.55	49.24	49.18	49.50	48.95
Al_2O_3	0.00	0.12	0.00	0.45	0.08	0.00	0.00	0.00	0.00	0.00	0.00	0.00	0.00	0.00	0.00	0.00
SO_3	30.99	30.70	30.92	31.47	29.32	31.23	32.20	31.66	31.94	31.98	33.11	32.66	32.91	33.00	32.88	33.29
P_2O_5	0.47	1.39	0.72	0.59	1.83	0.60	0.23	0.25	0.64	0.44	0.00	0.21	0.31	0.27	0.18	0.17
As_2O_5	0.25	0.00	0.00	0.29	0.00	0.00	0.00	0.00	0.00	0.00	0.00	0.00	0.00	0.00	0.00	0.00
H_2O^*	10.83	10.50	10.54	10.49	10.44	10.69	10.54	10.50	10.85	10.67	11.04	11.19	11.01	10.99	11.16	10.92
total	99.38	98.64	98.38	99.17	97.01	98.89	98.53	96.90	99.21	98.18	99.23	99.57	99.30	99.36	99.92	99.73
Na	0.000	0.000	0.015	0.029	0.025	0.117	0.438	0.414	0.435	0.422	0.918	0.916	0.879	0.861	0.826	0.804
K	0.943	0.891	0.951	0.945	0.879	0.845	0.570	0.519	0.463	0.474	0.006	0.013	0.017	0.038	0.087	0.108
Ca	0.000	0.004	0.000	0.000	0.005	0.000	0.000	0.000	0.000	0.004	0.000	0.000	0.000	0.000	0.005	0.011
H_3O^+	0.057	0.104	0.034	0.026	0.091	0.038	0.000	0.066	0.102	0.100	0.076	0.071	0.103	0.101	0.081	0.077
Σ *A*-site	1.000	1.000	1.000	1.000	1.000	1.000	1.008	1.000	1.000	1.000	1.000	1.000	1.000	1.000	1.000	1.000
Fe	3.040	2.947	2.985	2.897	3.005	2.999	2.927	2.954	2.983	2.955	2.976	3.021	2.969	2.961	3.001	2.932
Al	0.000	0.012	0.000	0.044	0.008	0.000	0.000	0.000	0.000	0.000	0.000	0.000	0.000	0.000	0.000	0.000
Σ *B*-site	3.040	2.959	2.985	2.940	3.013	2.999	2.927	2.954	2.983	2.955	2.976	3.021	2.969	2.961	3.001	2.932
S	1.956	1.903	1.949	1.946	1.868	1.958	1.984	1.982	1.956	1.969	2.000	1.986	1.979	1.982	1.988	1.989
P	0.033	0.097	0.051	0.041	0.132	0.042	0.016	0.018	0.044	0.031	0.000	0.014	0.021	0.018	0.012	0.011
As	0.011	0.000	0.000	0.012	0.000	0.000	0.000	0.000	0.000	0.000	0.000	0.000	0.000	0.000	0.000	0.000
Σ *X*-site	2.000	2.000	2.000	2.000	2.000	2.000	2.000	2.000	2.000	2.000	2.000	2.000	2.000	2.000	2.000	2.000
OH	6.077	5.784	5.903	5.768	5.912	5.956	5.772	5.844	5.904	5.840	5.929	6.048	5.886	5.866	5.995	5.795

Apfu on the base P+As+S = 2; H_2O^* contents were calculated based on charge balance and filling the *A* position with the theoretical H_3O^+ content up to the sum of 1 *pfu*.

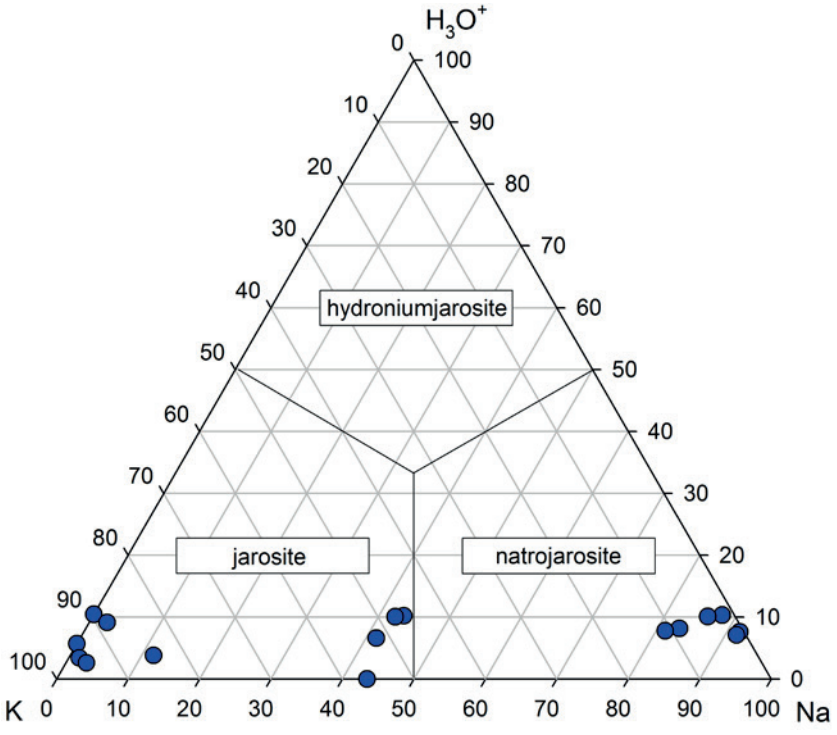

Fig. 8 *Ternary diagram of alunite group minerals from Laurion.*

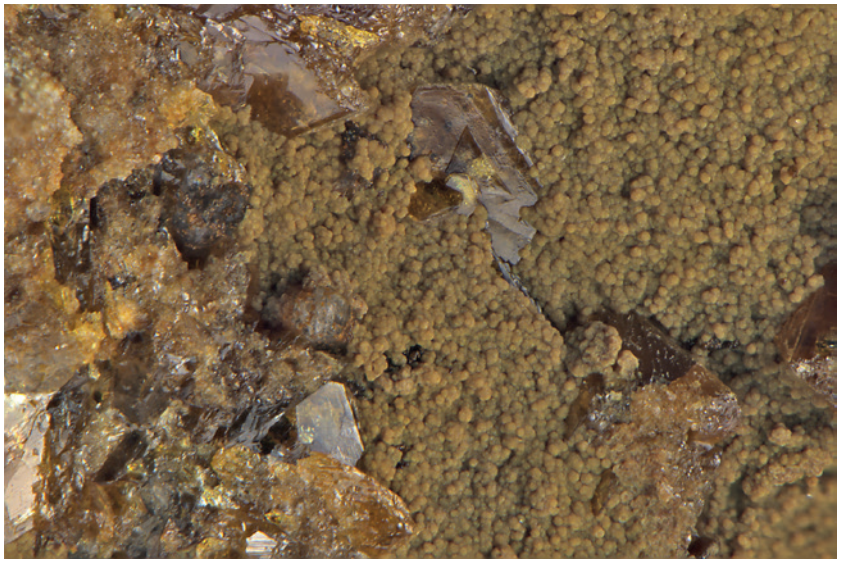

Fig. 9 *Crust of spherical aggregates of mitridatite with orange-brown crystals of jarosite-natrojarosite. FOV 1.9 mm. Photo by L. Vrtiška.*

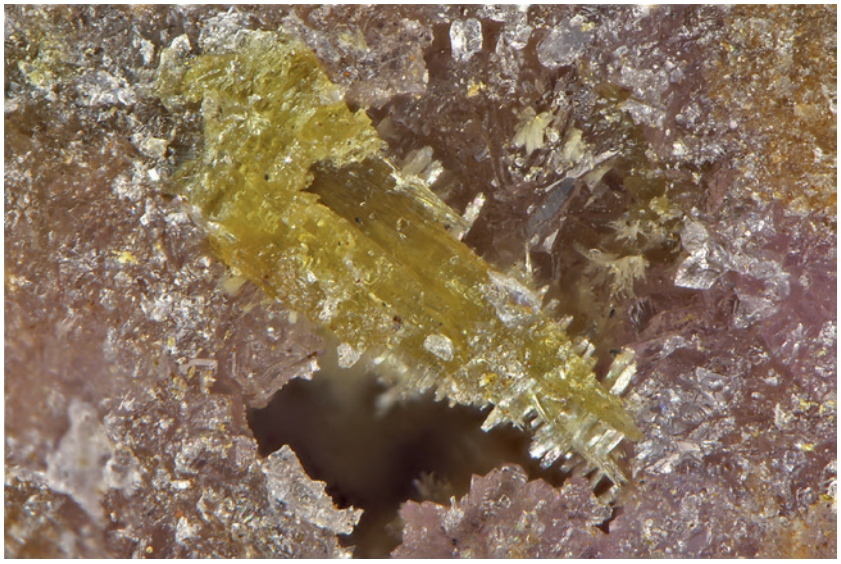

Fig. 10 *Perpendicularly clustered crystals of yellow jahnsite-(NaFeMg) on pink phosphosiderite. FOV 2.2 mm. Photo by L. Vrtiška.*

Fig. 11 *Crystals of yellow jahnsite-(NaFeMg) with orange-brown jarosite-natrojarosite and pink phosphosiderite. FOV 3.5 mm. Photo by L. Vrtiška.*

Jarosite-natrojarosite series

Amber yellow, dark orange to orange-brown tabular crystals of jarosite and natrojarosite up to 3 mm in size grow on the phosphosiderite (Fig. 7). Jarosite and natrojarosite crystals often form rosette-like aggregates.

Minerals of the alunite group (jarosite and natrojarosite) show a distinct zonality in the BSE (Figs. 4, 6). Based on the study of the chemical composition, three groups of data are distinguished in Table 4. These groups include jarosite, natrojarosite and intermediate members near the jarosite-natrojarosite boundary (Fig. 8). The affiliation of the minerals to the alunite group was verified by PXRD analysis. However, the individual zones are thin and for this reason it was not possible to obtain sufficient material for PXRD analysis of the individual members. The results of the PXRD study are therefore mixed records of two mineral phases and were not suitable for refinement of the unit-cell parameters.

The study of the chemical composition of **jarosite**, with the ideal chemical formula $AB^{3+}{}_3(XO_4)_2(OH)_6$, revealed the dominant occupation of the cationic *A*-site by K (Fig. 8), with minor contents of Na (up to 0.12 *apfu*), Ca (up to 0.01 *apfu*) and calculated contents of H_3O^+ (in the range of 0.03 - 0.10 *pfu*). The *B*-site is dominated by Fe^{3+} with small contents of Al (up to 0.04 *apfu*). The tetrahedral *X*-site is dominantly occupied by S with elevated P (up to 0.13 *apfu*) and As (up to 0.01 *apfu*) contents. The empirical formula of jarosite from Lavrion (mean of 6 analyses) based on S+P+As = 2 *apfu* is $[K_{0.91}Na_{0.03}(H_3O)_{0.06}]_{\Sigma 1.00}(Fe^{3+}{}_{2.98}Al_{0.01})_{\Sigma 2.99}[(SO_4)_{1.93}(PO_4)_{0.07}]_{\Sigma 2.00}(OH)_{5.90}$.

Natrojarosite in the studied samples from the Lavrion contains predominantly Na in the *A*-site (Fig. 8), with minor contents of K (0.01 - 0.11 *apfu*), Ca (up to 0.01 *apfu*) and calculated H_3O^+ contents (in the range of 0.07 - 0.10 *pfu*). The *B*-site is occupied only by Fe^{3+}. The *X*-site is dominantly occupied by S with elevated P (up to 0.02 *apfu*) contents. The empirical formula of natrojarosite from Lavrion (mean of 6 analyses) based on S+P = 2 *apfu* is $[Na_{0.88}K_{0.04}(H_3O)_{0.08}]_{\Sigma 1.00}Fe^{3+}{}_{2.98}[(SO_4)_{1.99}(PO_4)_{0.01}]_{\Sigma 2.00}(OH)_{5.92}$.

The study of chemical composition of intermediate members near the **jarosite-natrojarosite** boundary revealed a slight predominance of K (0.46 - 0.57 *apfu*) over Na (0.41 -

0.44 *apfu*) in the *A*-site and minor contents of Ca (up to 0.004 *apfu*) and calculated H_3O^+ contents (in the range of 0.00 - 0.10 *pfu*) in this structural position (Fig. 8). All these members formally belong to the jarosite field. The *B*-site is occupied only by Fe^{3+}. The *X*-site is dominantly occupied by S with elevated P (up to 0.04 *apfu*) contents. The empirical formula of these intermediate members (mean of 4 analyses) based on S+P = 2 *apfu* is $[K_{0.51}Na_{0.43}(H_3O)_{0.06}]_{\Sigma 1.00}Fe^{3+}_{2.96}[(SO_4)_{1.97}(PO_4)_{0.03}]_{\Sigma 2.00}(OH)_{5.84}$.

Table 5 *Chemical composition of mitridatite from Lavrion (wt. %)*

	mean	1	2	3	4	5	6	7	8	9
K_2O	0.19	0.17	0.19	0.24	0.22	0.17	0.19	0.19	0.16	0.17
CaO	14.03	13.74	14.41	16.91	13.65	13.42	13.98	12.82	13.06	14.27
MgO	0.25	0.29	0.31	0.32	0.24	0.30	0.23	0.20	0.14	0.26
Fe_2O_3	26.01	26.54	27.21	31.01	24.27	24.68	25.42	24.31	24.06	26.58
P_2O_5	24.16	23.35	24.38	29.26	22.89	23.24	24.12	22.70	22.79	24.74
As_2O_5	2.78	2.54	3.05	3.31	2.72	2.80	2.87	2.34	2.60	2.80
SO_3	0.20	0.26	0.20	0.18	0.21	0.20	0.11	0.24	0.19	0.19
H_2O*	6.61	6.38	6.71	7.99	6.28	6.38	6.60	6.18	6.24	6.76
total	74.24	73.27	76.46	89.22	70.48	71.19	73.52	68.98	69.24	75.77
K	0.033	0.031	0.032	0.034	0.040	0.031	0.033	0.035	0.029	0.029
Ca	2.044	2.074	2.069	2.041	2.093	2.026	2.042	1.998	2.019	2.034
Mg	0.052	0.061	0.062	0.054	0.051	0.063	0.047	0.043	0.030	0.052
Fe	2.662	2.814	2.744	2.628	2.614	2.617	2.608	2.661	2.612	2.661
Σ	4.790	4.980	4.908	4.757	4.799	4.737	4.730	4.738	4.690	4.775
P	2.782	2.785	2.766	2.790	2.774	2.773	2.784	2.796	2.783	2.786
As	0.198	0.187	0.214	0.195	0.204	0.206	0.205	0.178	0.196	0.195
S	0.020	0.027	0.020	0.015	0.023	0.021	0.011	0.026	0.021	0.019
Σ	3.000	3.000	3.000	3.000	3.000	3.000	3.000	3.000	3.000	3.000
H_2O	3.000	3.000	3.000	3.000	3.000	3.000	3.000	3.000	3.000	3.000

Mean of 9 point analyses; *apfu* on the base P+As+S = 3; H_2O* was calculated based on the ideal content of 3 water molecules *pfu*.

Table 6 *X-ray powder diffraction data of jahnsite-(NaFeMg) from Lavrion*

h	*k*	*l*	d_{obs}	I_{obs}	d_{calc}	*h*	*k*	*l*	d_{obs}	I_{obs}	d_{calc}	*h*	*k*	*l*	d_{obs}	I_{obs}	d_{calc}
0	0	1	9.284	100	9.246	2	1	2	3.046	1	3.040	3	2	3	1.8972	<1	1.8974
0	1	0	7.173	1	7.140	4	0	1	2.971	3	2.971	0	3	3	1.8801	<1	1.8813
2	0	0	7.055	<1	7.067	-1	1	3	2.960	2	2.955	-5	2	4	1.8722	1	1.8740
-2	0	1	6.881	<1	6.889	-4	0	3	2.864	1	2.867	-1	1	5	1.8482	<1	1.8500
1	1	0	6.393	1	6.373	-2	2	2	2.834	1	2.838	5	3	0	1.8194	<1	1.8206
-1	1	1	5.691	1	5.677	5	1	0	2.625	1	2.628	6	1	2	1.7947	1	1.7924
2	1	0	5.029	2	5.023	-4	2	1	2.5921	2	2.5917	7	2	0	1.7573	1	1.7576
1	1	1	4.911	8	4.893	-2	2	3	2.4072	<1	2.4092	-5	3	3	1.7484	<1	1.7482
2	0	1	4.854	<1	4.849	-6	1	2	2.3406	1	2.3405	5	3	1	1.7139	<1	1.7143
0	0	2	4.626	13	4.608	-6	0	3	2.2971	<1	2.2964	3	4	0	1.6701	<1	1.6692
-3	1	1	4.061	1	4.071	2	3	0	2.2558	<1	2.2554	4	1	4	1.6339	<1	1.6354
2	1	1	4.013	<1	4.012	-6	2	1	2.0479	<1	2.0487	-8	0	5	1.5802	<1	1.5808
3	1	0	3.934	<1	3.932	4	2	2	2.0076	2	2.0058	-3	4	3	1.5492	<1	1.5493
-4	0	0	3.536	1	3.534	3	3	1	2.0028	2	2.0021	0	4	3	1.5443	1	1.5433
-4	0	2	3.436	1	3.445	-6	1	4	1.9624	<1	1.9631	7	3	0	1.5403	1	1.5397
-1	2	1	3.338	<1	3.335	-4	3	2	1.9579	1	1.9580	-7	2	5	1.5238	<1	1.5243
3	1	1	3.286	2	3.287	2	3	2	1.9399	3	1.9421	8	0	2	1.4866	<1	1.4854
2	2	0	3.182	1	3.186	4	1	3	1.9249	<1	1.9244	-8	2	5	1.4450	<1	1.4454
0	0	3	3.083	1	3.072												

Table 7 *Unit-cell parameters of jahnsite-(NaFeMg) (for monoclinic space group P2/a)*

	this paper	Kampf et al. (2008)
a [Å]	15.085(4)	15.0811(16)
b [Å]	7.140(2)	7.1403(8)
c [Å]	9.835(3)	9.8299(11)
β [°]	110.45(4)	110.445(1)
V [Å^3]	992.5(5)	991.8(2)

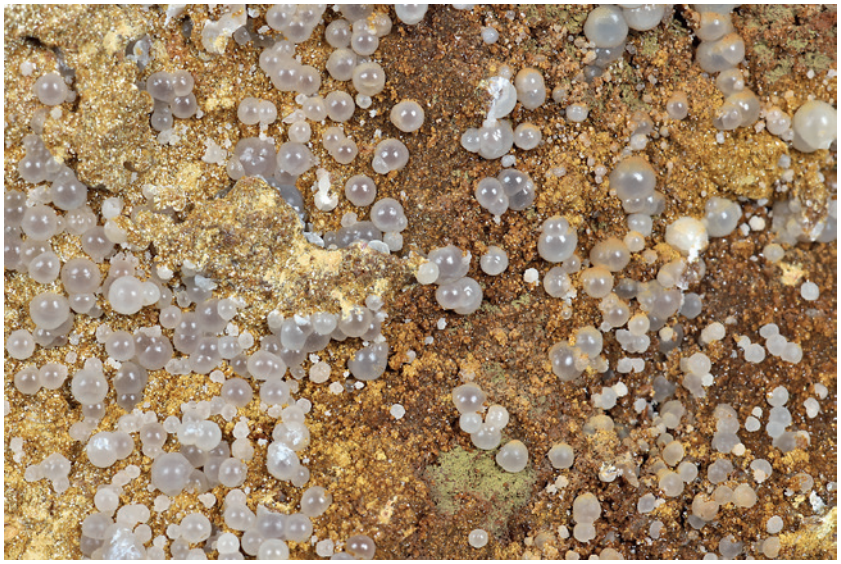

Fig. 12 *Concentric spherical aggregates of fluorapatite on jarosite-natrojarosite. FOV 35 mm. Photo by L. Vrtiška.*

Fig. 13 *Concentric spherical aggregates of fluorapatite. FOV 14 mm. Photo by L. Vrtiška.*

Fig. 14 *Spherical aggregate of fluorapatite composed of clear columnar crystals. FOV 1.2 mm. Photo by L. Vrtiška.*

Mitridatite

Mitridatite was observed as olive-green, yellow-green to yellow-brown powdery coatings and spherical aggregates up to 0.0X mm in size (Fig. 9).

Due to the difficulty in separating a sufficient amount of pure material, it was not possible to verify the mitridatite by PXRD analysis. The study of the chemical composition of mitridatite (Table 5), a mineral with the ideal formula $Ca_2Fe^{3+}{}_3(PO_4)_3O_2{\cdot}3H_2O$, revealed a dominant Ca (2.00 - 2.09 *apfu*) and Fe^{3+} (2.61 - 2.88 *apfu*) accompanied by elevated Mg (up to 0.32 *apfu*) and K (up to 0.24 *apfu*) contents. The tetrahedral position is dominated by P in range of 2.77 - 2.79 *apfu* with elevated As (up to 0.21 *apfu*) and minor S (up to 0.03 *apfu*) contents. The empirical formula of mitridatite from Lavrion (average of nine point analyses) can be expressed as $(Ca_{2.04}K_{0.03}Mg_{0.05}Fe^{3+}{}_{2.66})_{\Sigma 4.78}[(PO_4)_{2.78}(AsO_4)_{0.20}(SO_4)_{0.02}]_{\Sigma 3.00}O_2{\cdot}3H_2O$ based on P+As+S = 3 *apfu*. The large deficiency in the sum of oxides is probably due to the significant porosity of the studied samples.

Jahnsite-(NaFeMg)

Jahnsite-(NaFeMg) forms translucent vitreous deep yellow elongated crystals with striations parallel to [010]. The crystals form subparallel, divergent and perpendicular intergrowths and clusters up to 2 mm in size (Figs. 10, 11). Crystals of jahnsite-(NaFeMg) in some places completely fill the cavities with jarosite and phosphosiderite.

Jahnsite was first described by Moore (1974) and its crystal structure was determined by Moore and Araki (1974). Moore and Ito (1978) recognized that a variety of cation substitutions were possible in the jahnsite structure type. They suggested the general formula $XM1M2_2M3_2(H_2O)_8(OH)_2(PO_4)_4$, where the *X* site accommodates the largest cations, the *M*1 and *M*2 sites accommodate medium- to small-sized octahedrally coordinated cations (e.g. Mn^{2+}, Fe^{2+}, Fe^{3+} and Mg^{2+}) and the *M*3 site accommodates the small octahedrally coordinated cations Fe^{3+} or Al^{3+}. They proposed a naming scheme in which the root name jahnsite is applied to minerals with *M*3 = Fe^{3+} and whiteite to those with *M*3 = Al^{3+}; the root name is then followed by a suffix of the form -(*XM*1*M*2). Note that the minerals keckite and rittmannite do not conform to the naming

scheme proposed by Moore and Ito (1978). Further to the definition of jahnsite-group minerals for which structure analysis is not possible, Moore and Ito (1978) recommended that ‘‘tentative distributions of cations proceed from ionic radii arguments where the radius increases *M*3 < *M*2 < *M*1 < *X*“. All but one subsequent structure refinement has borne this out (cf. Grey et al. 2010; Capitelli et al. 2011; Yakovenchuk et al. 2012; Elliott 2016; Kampf et

Table 8 *Chemical composition of jahnsite-(NaFeMg) from Lavrion (wt. %)*

	mean	1	2	3	4	5	6	7	8	9	10	11	12	13	14
Na_2O	2.66	2.57	2.55	2.67	2.67	2.76	2.86	2.68	3.02	2.48	2.52	2.56	2.64	2.72	2.52
CaO	1.14	1.63	1.60	1.45	1.30	0.78	0.42	0.56	1.06	1.37	1.37	1.45	0.94	0.86	1.13
MgO	11.41	10.78	11.45	11.72	11.52	10.33	11.04	10.89	11.18	11.80	12.34	11.65	11.98	11.53	11.59
*FeO	0.20	0.17	0.00	0.00	0.00	1.07	0.12	0.76	0.00	0.07	0.00	0.27	0.00	0.00	0.36
$*Fe_2O_3$	27.86	27.64	27.03	27.95	27.85	27.91	29.04	27.79	28.04	27.77	27.02	27.54	27.95	28.27	28.23
P_2O_5	36.43	36.17	36.17	36.89	36.58	35.57	36.73	35.38	36.16	36.82	36.04	35.89	37.26	37.19	37.21
As_2O_5	2.70	1.94	3.16	2.78	3.46	2.26	2.90	2.83	2.56	1.91	3.55	2.17	3.23	2.66	2.32
$**H_2O$	19.34	18.97	19.35	19.60	19.66	18.77	19.56	18.85	19.16	19.29	19.41	18.90	19.93	19.71	19.62
total	101.74	99.87	101.31	103.06	103.04	99.44	102.66	99.73	101.18	101.50	102.25	100.43	103.93	102.94	102.98
Na	0.639	0.630	0.613	0.634	0.632	0.684	0.680	0.661	0.733	0.598	0.604	0.630	0.616	0.642	0.597
Ca	0.151	0.221	0.212	0.190	0.170	0.107	0.055	0.076	0.142	0.183	0.181	0.197	0.121	0.112	0.148
Σ*X*	0.790	0.851	0.825	0.824	0.802	0.791	0.735	0.738	0.875	0.780	0.785	0.827	0.737	0.754	0.745
Fe^{3+}	0.598	0.630	0.521	0.574	0.558	0.652	0.680	0.661	0.642	0.598	0.513	0.630	0.532	0.588	0.597
Fe^{2+}	0.021	0.018	0.000	0.000	0.000	0.114	0.012	0.081	0.000	0.007	0.000	0.029	0.000	0.000	0.037
Mg	0.112	0.032	0.116	0.138	0.096	0.000	0.019	0.066	0.087	0.187	0.273	0.204	0.150	0.091	0.113
Σ*M1*	0.732	0.680	0.637	0.712	0.653	0.766	0.711	0.808	0.728	0.792	0.786	0.863	0.681	0.680	0.747
Mg	1.998	2.000	2.000	2.000	2.000	1.968	2.000	2.000	2.000	2.000	2.000	2.000	2.000	2.000	2.000
Fe^{3+}	0.002	0.000	0.000	0.000	0.000	0.032	0.000	0.000	0.000	0.000	0.000	0.000	0.000	0.000	0.000
Σ*M2*	2.000	2.000	2.000	2.000	2.000	2.000	2.000	2.000	2.000	2.000	2.000	2.000	2.000	2.000	2.000
Fe^{3+}	2.000	2.000	2.000	2.000	2.000	2.000	2.000	2.000	2.000	2.000	2.000	2.000	2.000	2.000	2.000
Σ*M3*	2.000	2.000	2.000	2.000	2.000	2.000	2.000	2.000	2.000	2.000	2.000	2.000	2.000	2.000	2.000
P	3.825	3.872	3.795	3.822	3.779	3.849	3.814	3.812	3.832	3.876	3.771	3.856	3.797	3.831	3.852
As	0.175	0.128	0.205	0.178	0.221	0.151	0.186	0.188	0.168	0.124	0.229	0.144	0.203	0.169	0.148
Σ*D*	4.000	4.000	4.000	4.000	4.000	4.000	4.000	4.000	4.000	4.000	4.000	4.000	4.000	4.000	4.000
OH	1.004	1.061	0.832	1.012	0.836	1.114	0.893	1.095	1.115	1.145	1.052	1.380	0.752	0.814	0.984
H_2O	8.000	8.000	8.000	8.000	8.000	8.000	8.000	8.000	8.000	8.000	8.000	8.000	8.000	8.000	8.000

Mean of 14 point analyses; *apfu* on the base P+As = 4; * FeO and $*Fe_2O_3$: the *M*1 position in jahnsite-group minerals is preferentially occupied by Fe^{2+} in most cases. In the case of the monovalent Na content in the *X* position, it is balanced by an appropriate amount of Fe^{3+} in the *M*1 position, the remaining Fe is assumed to be divalent. $**H_2O$ was calculated based on the ideal content of 8 water molecules *pfu* and charge balance.

Table 9 *X-ray powder diffraction data of fluorapatite from Lavrion*

h	*k*	*l*	d_{obs}	I_{obs}	d_{calc}	*h*	*k*	*l*	d_{obs}	I_{obs}	d_{calc}	*h*	*k*	*l*	d_{obs}	I_{obs}	d_{calc}
0	1	0	8.093	9	8.096	1	3	0	2.2439	37	2.2438	1	4	1	1.7103	<1	1.7102
0	1	1	5.242	1	5.245	0	1	3	2.2108	<1	2.2100	2	3	2	1.6337	2	1.6341
1	1	0	4.672	1	4.674	1	3	1	2.1339	3	2.1335	1	1	4	1.6209	<1	1.6165
0	2	0	4.045	10	4.045	1	1	3	2.0601	1	2.0615	1	3	3	1.6052	<1	1.6052
1	1	1	3.865	1	3.867	0	4	0	2.0236	1	2.0225	0	5	1	1.5751	<1	1.5752
0	0	2	3.442	3	3.446	0	2	3	1.9959	1	1.9977	3	3	0	1.5571	<1	1.5569
0	1	2	3.168	1	3.170	2	2	2	1.9332	7	1.9333	2	4	0	1.5296	2	1.5289
1	2	0	3.058	29	3.058	1	3	2	1.8804	4	1.8803	3	3	1	1.5189	<1	1.5187
1	2	1	2.795	44	2.795	2	3	0	1.8570	5	1.8560	2	4	1	1.4934	<1	1.4926
1	1	2	2.771	8	2.773	1	2	3	1.8361	5	1.8367	0	5	2	1.4653	3	1.4646
0	3	0	2.697	100	2.697	2	3	1	1.7934	9	1.7921	0	3	4	1.4535	<1	1.4520
0	2	2	2.622	4	2.623	1	4	0	1.7659	19	1.7654	1	5	0	1.4506	<1	1.4530
0	3	1	2.5105	3	2.5113	0	4	2	1.7441	6	1.7443	1	5	1	1.4187	4	1.4218
2	2	0	2.3361	<1	2.3354	0	0	4	1.7210	1	1.7230	1	4	3	1.3977	<1	1.3998
1	2	2	2.2857	1	2.2872												

Table 10 *Unit-cell parameters of fluorapatite (for hexagonal space group $P6_3/m$)*

	this paper	Perdikatsis (1991)
a [Å]	9.342(4)	9.3207(5)
c [Å]	6.8921(3)	6.8947(5)
V [Å^3]	520.9(3)	518.73

Fig. 15 *Spray clusters of colorless fluorapatite crystals with light pink phosphosiderite and orange-brown jarosite-natrojarosite. FOV 2.2 mm. Photo by L. Vrtiška.*

Fig. 16 *Translucent irregular crystals of collinsite growing on white spherical aggregates of fluorapatite. FOV 20 mm. Photo by L. Vrtiška.*

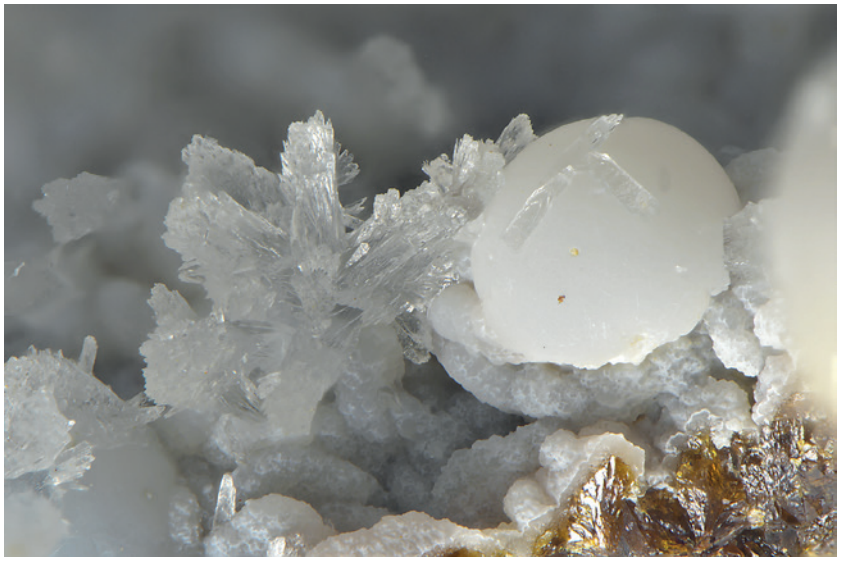

Fig. 17 *Transparent irregular crystals of collinsite growing on white spherical aggregates of fluorapatite. FOV 3 mm. Photo by L. Vrtiška.*

al. 2016). The exception was jahnsite-(NaFeMg), for which Kampf et al. (2008) found the *M*1 and *M*2 sites to be very similar in size and reversed from the "normal" sequence, with *M*1 < *M*2. In practice, because jahnsite-group minerals usually occur in crystals unsuitable for single-crystal study, the cation size argument of Moore and Ito (1978) has been applied in defining all jahnsite group minerals for which structure refinements were not possible; the continuation of this approach seems justified. The foregoing discussion was approved by the Commission on New Minerals Nomenclature and Classification (CNMNC) of the International Mineralogical Association (IMA) as the basis for the formal establishment of the jahnsite group.

The peak positions in experimental X-ray powder patterns of jahnsite-(NaFeMg) from Lavrion (Table 6) fit well with data published for this mineral from the type locality Tip Top mine in South Dakota, USA (Kampf et al. 2008). The refined unit-cell parameters, compared with published data, are given in the Table 7.

Chemical composition of jahnsite-(NaFeMg) is shown in Table 8. In the *M*3 position only Fe^{3+} was detected. The *M*2 position is dominantly occupied by Mg (1.97 - 2.00 *apfu*), and minor contents of Fe^{3+} (up to 0.03 *apfu*). The *M*1 position is occupied dominantly by Fe^{3+} (0.51 - 0.68 *apfu*) with increased Mg (up to 0.20 *apfu*) and minor Fe^{2+} (up to 0.11 *apfu*). Position *X* contains Na (0.60 - 0.73 *apfu*) and Ca (0.06 - 0.22 *apfu*). In addition to P, elevated As (0.12 - 0.23 *apfu*) concentrations were identified in the oxoanionic position. The average empirical formula of the jahnsite-(NaFeMg) (mean of 14 point analyses) was determined to be $(Na_{0.64}Ca_{0.15})_{\Sigma 0.79}(Fe^{3+}_{0.60}Fe^{2+}_{0.02}Mg_{0.11})_{\Sigma 0.73}(Mg)_{2.00}(Fe^{3+})_{\Sigma 2.00}[(PO_4)_{3.83}(AsO_4)_{0.17}]_{\Sigma 4.00}(OH)_{1.00}\cdot 8H_2O$. Low water contents may be due to dehydration of the sample during WDS analysis.

Fluorapatite

Fluorapatite occurs as white to light grey concentric spherical aggregates up to 4 mm in size (Figs. 12, 13) or forms white to colorless spherical aggregates composed of clear columnar or needle-like crystals up to 1 mm in size (Fig. 14). More rarely, it forms solitary clear columnar crystals and their spray clusters (Fig. 15). The peak positions in experimental X-ray powder patterns of fluorapatite from Lavrion (Table 9) agree well with data

published for carbonate-rich fluorapatite from the Epirus ore deposit in Greece (Perdikatsis 1991). The refined unit-cell parameters, compared with published data, are given in Table 10.

In addition to Ca and P, the chemical composition of fluorapatite (Table 11) showed elevated levels of Zn (up to 0.17 *apfu*), Mg (up to 0.07 *apfu*) and S (up to 0.02 *apfu*). Some of the analyses are characterized by a deficit of elements in the structural position of phosphorus. This deficit is compensated by the calculated C content (0.00 -

Table 11 *Chemical composition of fluorapatite from Lavrion (wt. %)*

	mean	1	2	3	4	5	6	7	8
CaO	50.47	52.09	51.94	50.48	50.18	48.25	52.52	48.71	49.62
MgO	0.17	0.17	0.04	0.22	0.00	0.00	0.00	0.45	0.48
ZnO	1.21	0.88	1.32	0.00	1.82	2.45	0.43	1.44	1.34
P_2O_5	38.61	39.11	39.92	38.05	38.24	37.65	38.67	38.94	38.31
SO_3	0.13	0.35	0.36	0.00	0.00	0.00	0.00	0.12	0.20
CO_2*	0.26	0.48	0.00	0.32	0.51	0.17	0.89	0.00	0.25
F	3.85	3.91	3.70	4.25	3.50	3.64	3.92	3.86	4.02
F=-O	-1.62	-1.65	-1.56	-1.79	-1.47	-1.53	-1.65	-1.63	-1.69
total	93.08	95.34	95.72	91.53	92.77	90.63	94.78	91.89	92.53
Ca^{2+}	4.896	4.920	4.909	4.970	4.878	4.831	4.972	4.839	4.845
Mg^{2+}	0.023	0.022	0.005	0.030	0.000	0.000	0.000	0.062	0.065
Zn^{2+}	0.081	0.057	0.086	0.000	0.122	0.169	0.028	0.099	0.090
Σ	5.000	5.000	5.000	5.000	5.000	5.000	5.000	5.000	5.000
P^{5+}	2.959	2.919	2.981	2.960	2.937	2.979	2.893	3.057	2.955
S^{4+}	0.009	0.023	0.024	0.000	0.000	0.000	0.000	0.008	0.014
C^{4+}	0.032	0.058	0.000	0.040	0.063	0.021	0.107	0.000	0.031
Σ	3.000	3.000	3.005	3.000	3.000	3.000	3.000	3.065	3.000
F^-	1.102	1.095	1.032	1.235	1.004	1.076	1.095	1.132	1.159

Mean of 8 point analyses; *apfu* on the base Ca+Mg+Zn = 5; CO_2* was calculated based on P+S+C = 3 *apfu*.

Table 12 *X-ray powder diffraction data of collinsite from Lavrion*

h	*k*	*l*	d_{obs}	I_{obs}	d_{calc}	*h*	*k*	*l*	d_{obs}	I_{obs}	d_{calc}	*h*	*k*	*l*	d_{obs}	I_{obs}	d_{calc}
0	-1	0	6.288	21	6.279	-2	2	1	2.3673	3	2.3672	-2	-2	0	1.6980	4	1.6982
0	0	1	5.013	9	5.006	-2	-1	1	2.2901	8	2.2898	-1	1	3	1.6692	5	1.6700
-1	0	1	4.516	12	4.513	-1	3	0	2.2388	10	2.2385	1	-4	1	1.6622	8	1.6622
-1	1	1	3.852	1	3.849	-2	1	2	2.1937	6	2.1936	0	-2	3	1.6510	1	1.6501
0	1	1	3.516	8	3.518	0	1	2	2.1516	1	2.1512	-3	3	1	1.6376	1	1.6379
-1	-1	1	3.506	13	3.505	0	-3	1	2.1252	2	2.1248	2	-2	2	1.6170	<1	1.6166
1	-2	0	3.240	12	3.240	-1	-2	2	2.1162	15	2.1157	-3	-1	2	1.5950	1	1.5953
0	2	0	3.141	100	3.140	0	-3	0	2.0926	3	2.0931	0	-4	0	1.5701	4	1.5698
1	0	1	3.041	26	3.038	-2	-1	2	2.0613	8	2.0601	-2	4	1	1.5357	3	1.5359
0	-2	1	3.013	23	3.012	-2	3	0	2.0060	2	2.0060	-2	-2	3	1.5173	2	1.5166
-2	1	1	2.755	<1	2.754	1	-2	2	1.9927	2	1.9924	0	-4	2	1.5050	2	1.5059
1	-2	1	2.736	8	2.735	1	0	2	1.9700	9	1.9699	1	-2	3	1.4900	1	1.4908
-2	1	0	2.713	18	2.715	-2	2	2	1.9274	<1	1.9245	3	-3	1	1.4788	<1	1.4789
-1	2	1	2.706	28	2.705	1	2	1	1.8711	8	1.8702	-1	-3	3	1.4649	1	1.4667
-1	0	2	2.682	63	2.681	-2	-2	1	1.8382	5	1.8372	-4	2	1	1.4213	<1	1.4213
0	-1	2	2.5511	2	2.5493	-3	2	1	1.8320	6	1.8321	-4	1	2	1.4004	4	1.4001
-2	0	0	2.5375	3	2.5378	-1	0	3	1.7981	2	1.7988	2	-4	2	1.3682	2	1.3675
-1	-2	1	2.4673	7	2.4661	0	3	1	1.7833	2	1.7822	-4	0	1	1.3570	1	1.3577
-1	1	2	2.4039	5	2.4033	0	2	2	1.7573	2	1.7588	-2	4	2	1.3518	1	1.3526

Table 13 *Unit-cell parameters of collinsite (for triclinic space group P-1)*

	this paper	Brotherton et al. (1974)
a [Å]	5.737(2)	5.7344(8)
b [Å]	6.781(2)	6.780(1)
c [Å]	5.4474(19)	5.4413(9)
α [°]	97.27(3)	97.29(1)
β [°]	108.61(3)	108.56(1)
γ [°]	107.26(3)	107.28(1)
V [Å^3]	185.9(1)	185.69

Table 14 *Chemical composition of collinsite from Lavrion (wt. %)*

	mean	1	2	3	4	5	6
CaO	33.99	33.06	34.13	34.74	33.37	34.26	34.37
MgO	10.21	10.62	9.92	9.86	10.65	10.11	10.11
Al_2O_3	0.02	0.00	0.05	0.06	0.00	0.00	0.00
P_2O_5	41.49	41.24	42.06	41.46	41.24	41.23	41.71
H_2O*	10.53	10.47	10.68	10.52	10.47	10.47	10.59
total	96.24	95.39	96.84	96.64	95.73	96.07	96.78
Ca	2.074	2.029	2.054	2.121	2.048	2.103	2.086
Mg	0.867	0.907	0.831	0.838	0.909	0.864	0.854
Al	0.002	0.000	0.003	0.004	0.000	0.000	0.000
Σ	2.943	2.936	2.888	2.963	2.958	2.967	2.939
P	2.000	2.000	2.000	2.000	2.000	2.000	2.000
H_2O	2.000	2.000	2.000	2.000	2.000	2.000	2.000

Mean of 6 point analyses; *apfu* on the base P = 2; H_2O* was calculated based on the ideal content of 2 water molecules *pfu*.

0.11 *apfu)*. The higher than theoretical F content (1 *apfu*) found in most analyses may be related to the orientation of the fluorapatite grains (Stormer et al. 1993). The empirical formula of fluorapatite from Lavrion (mean of 8 analyses) based on 5 *apfu* in the Ca structural position is $(Ca_{4.90}Zn_{0.08}Mg_{0.02})_{\Sigma 5.00}[(PO_4)_{2.96}(SO_4)_{0.01}(CO_3)_{0.03}]_{\Sigma 3.00}F_{1.10}$.

Collinsite

Collinsite forms white to colorless columnar and lanceolate crystals and their irregular aggregates up to 3 mm in size, growing on spherical aggregates of fluorapatite (Figs. 16, 17).

The peak positions in experimental X-ray powder patterns (Table 12) agree well with data published for collinsite from Milgun Station in Western Australia (Brotherton et al. 1974). The refined unit-cell parameters, compared with published data, are given in Table 13.

Chemical composition of studied sample (Table 14) agrees very well with the ideal formula of collinsite $Ca_2Mg(PO_4)_2 \cdot 2H_2O$. The cationic sites are occupied by dominant Ca and Mg with minor contents of Al (up to 0.004 *apfu*). The empirical formula of collinsite from Lavrion (mean of 6 analyses) based on P = 2 *apfu* is $Ca_{2.07}Mg_{0.88}(PO_4)_2 \cdot 2H_2O$.

Discussion

The Lavrion mine district is known for its large amount of supergene minerals, dominated by arsenates and sulphates. Phosphate minerals are rare at this locality and most of them belong to the alunite supergroup (e.g. plumbogummite, corkite, crandallite, gorceixite, goyazite, hinsdalite) or apatite group (e.g. fluorapatite, pyromorphite, phosphohedyphane; Möckel 2000; Kolitsch et al. 2014; Rieck et al. 2018; Ismagilova et al. 2022). Unusually large accumulations of phosphates, especially phosphosiderite in association with mitridatite, jahnsite-(NaFeMg), fluorapatite and collinsite, and sulphates from the alunite supergroup, jarosite and natrojarosite, studied in this work, have not been published from this deposit before. The occurrence of very rare jahnsite-(NaFeMg) is interesting, as it has only been described from four other localities in the world including the type locality (Tip Top Mine, South Dakota, USA; Kampf et al. 2008).

The activity of As and partly S in phosphorus-rich fluids is reflected in the chemical composition of most minerals of this association. Unusually elevated As contents were observed mainly in jahnsite-(NaFeMg), mitridatite, phosphosiderite and jarosite-natrojarosite. Slightly elevated S concentrations were observed in phosphosiderite, fluorapatite and mitridatite. The source of phosphorus for phosphate formation was not identified. No accumulation of primary phosphates has been reported from the deposit yet; it can be therefore assumed that P was rather leached from minerals in the surrounding rocks or it may be of biogenic origin. Documentary samples are stored in the mineralogical collection of the National Museum in Prague and in the private collection of Ivan Prachař.

Acknowledgements

The study was financially supported by the Ministry of Culture of the Czech Republic (long-term project DKRVO 2024-2028/1.II.b; National Museum, 00023272).

References

Bolanz RM, Wierzbicka-Wieczorek M, Giester G, Göttlicher J, Steininger R (2016) Structural incorporation of As^{5+} into phosphosiderite by a strengite/scorodite–like arrangement. ChemistrySELECT 1(14): 4152-4160

Brothernton PD, Maslen EN, Pryce MW, White AH (1974) Crystal structure of collinsite. Austr J Chem 27: 653-656

Capitelli F, Chita G, Cavallo A, Bellatreccia F, Ventura GD (2011) Crystal structure of whiteite-(CaFeMg) from Crosscut Creek, Canada. Z Krist 226: 731-738

Elliott P (2016) Jahnsite-(CaFeMg), a new mineral from Tom's quarry, South Australia: description and crystal structure. Eur J Mineral 28: 991-996

Fanfani L, Zanazzi PF (1966) La struttura cristallina della metastrengite. Atti della Accademia Nazionale dei Lincei, Classe di Scienze Fisiche, Matematiche e Naturali, Rendiconti Serie 8(40): 880-889

Grey IE, Mumme WG, Neville SM, Wilson NC, Birch WD (2010) Jahnsite - whiteite solid solutions and associated minerals in the phosphate pegmatite at Hagendorf-Süd, Bavaria, Germany. Mineral Mag 74(6): 969-978

Ismagilova RM, Rieck B, Kampf AR, Giester G, Zhitova ES, Lengauer CL, Krivovichev SV, Zolotarev AA, Ciesielczuk J, Mihkailova JA, Belakovsky JI, Bocharov VN, Shilovskikh VV, Vlasenko NS, Nash BP, Adams PM (2022) Goldhillite, $Cu_5Zn(AsO_4)_2(OH)_6·H_2O$, a new mineral species, and redefinition of philipsburgite, $Cu_5Zn[(AsO_4)(PO_4)](OH)_6·H_2O$, as an As–P ordered species. Mineral Mag 86(3): 436-446

Kampf AR, Steele IM, Loomis TA (2008) Jahnsite-(NaFeMg), a new mineral from the Tip Top mine, Custer County, South Dakota: Description and crystal structure. Amer Mineral 93: 940-945

Kampf AR, Adams PM, Nash BP (2016) Whiteite-(CaMgMg), $CaMg_3Al_2(PO_4)_4(OH)_2·8H_2O$, a new jahnsite-group mineral from the Northern Belle mine, Candelaria, Nevada, USA. Can Mineral 54: 1513-1523

Kolitsch U, Rieck B, Brandstätter F, Schreiber F, Fabritz KH, Blass G, Gröbner J (2014) Neufunde aus dem altem Bergbau und den Schlacken von Lavrion (I). Mineralien-Welt 25(1): 60-75

Laugier J, Bochu B (2011) LMGP-suite of programs for the interpretation of X-ray experiments. Accessed in April 2011 at http://www. ccp14.ac.uk/tutorial/lmgp

Marinos G, Petrascheck WE (1956) Laurium: Geological and geophysical research. Greece. Inst Geol Subsurf Res 4: 1-246

Möckel S (2000) Strashimirit und 11 weitere Neubestimmungen aus Lavrion (GR). Lapis 25(7-8): 74

Moore PB (1974) I. Jahnsite, segelerite, and robertsite, three new transition metal phosphate species II. Redefinition of overite, an isotype of segelerite III. Isotypy of robertsite, mitridatite, and arseniosiderite. Amer Mineral 59: 48-59

Moore PB, Araki T (1974) Jahnsite, $CaMn^{2+}Mg_2(H_2O)_8Fe^{3+}_2(OH)_2[PO_4]_4$: A novel stereoisomerism of ligands about octahedral corner-chains. Amer Mineral 59: 964-973

Moore PB, Ito J (1978) I. Whiteite, a new species, and a proposed nomenclature for the jahnsite-whiteite complex series. II. New data on xanthoxenite. III. Salmonsite discredited. Mineral Mag 42: 309-323

Perdikatsis B (1991) X-ray powder diffraction study of francolite by the Rietveld method. Material Science Forum 79: 809-814

Pouchou JL, Pichoir F (1985) "PAP" (φρZ) procedure for improved quantitative microanalysis. In: Armstrong JT (Ed) Microbeam Analysis: 104-106. San Francisco Press, San Francisco

Rieck B, Kolitsch U, Voudouris P, Giester G, Tzeferis P (2018) Weitere Neufunde aus Lavrion, Griechenland. Mineralien-Welt 29(5): 32-77

Stormer JC, Pierson MJ, Tacker RC (1993) Variation of F and Cl X-ray intensity due to anisotropic diffusion of apatite during electron microprobe analysis. Amer Mineral 78: 641-648

Voudouris P, Melfos V, Mavrogonatos C, Photiades A, Moraiti E, Rieck B, Kolitsch U, Tarantola A, Scheffer C, Morin D, Vanderhaeghe O, Spry PG, Ross J, Soukis K, Vaxevanopoulos M, Pekov IV, Chukanov NV, Magganas A, Kati M, Katerinopoulos A, Zaimis S (2021) The Lavrion mines: A unique site of geological and mineralogical heritage. Minerals 11(76): 1-22

Yakovenchuk VN, Keck E, Krivovichev SV, Pakhomovsky YA, Selivanova EA, Mikhailova JA, Chernyatieva AP, Ivanyuk GY (2012) Whiteite-(CaMnMn), $CaMnMn_2Al_2[PO_4]_4(OH)_2·8H_2O$, a new mineral from the Hagendorf-Süd granitic pegmatite, Germany. Mineral Mag 76(7): 2761-2771